Article

Not peer-reviewed version

A Novel Eu3+ Doped Glasses in the MoO3-WO3-La2O5- B2O3 System: Preparation, Structure and Photoluminescent Properties

Lyubomir Aleksandrov , Margarita Milanova * , Aneliya Yordanova , Reni Iordanova , Kenji Shinozaki , Tsuyoshi Honma , Takayuki Komatsu

Posted Date: 3 September 2024

doi: 10.20944/preprints202409.0145.v1

Keywords: glasses; structure; europium; photoluminescence

 doi:10.20944/preprints202409.0145.v1

Article

A Novel Eu^{3+} Doped Glasses in the MoO_3-WO_3-La_2O_5-B_2O_3 System: Preparation, Structure and Photoluminescent Properties

Lyubomir Aleksandrov [1], Margarita Milanova [1,*], Aneliya Yordanova [1], Reni Iordanova [1], Kenji Shinozaki [2], Tsuyoshi Honma [3] and Takayuki Komatsu [3]

[1] Institute of General and Inorganic Chemistry, Bulgarian Academy of Sciences, G. Bonchev, str. bld. 11, 1113 Sofia, Bulgaria; lubomirivov@gmail.com (L.A.); a.yordanova@svr.igic.bas.bg (A.Y.); reni@svr.igic.bas.bg (R.I.)

[2] National Institute of Advanced Industrial Science and Technology (AIST), 1-8-31 Midorigaoka, Ikeda, Osaka 563-8577, Japan; k-shinozaki@aist.go.jp

[3] Department of Materials Science and Technology, Nagaoka University of Technology, 1603-1 Kamitomioka-cho, Nagaoka 940-2188, Japan; honma@mst.nagaokaut.ac.jp (T.H.); komatsu@mst.nagaokaut.ac.jp (T.K.)

* Correspondence: margi@svr.igic.bas.bg

Abstract: A novel multicomponent glasses with nominal compositions of (50-x)MoO_3:xWO_3:25La_2O_3:25B_2O_3, x = 0, 10, 20, 30, 40, 50 mol% doped with 3 mol % Eu_2O_3 were prepared using a conventional melt quenching method. Their structure, thermal behavior and luminescent properties were investigated by Raman spectroscopy, differential thermal analysis and photoluminescence spectroscopy. Physical parameters as density, molar volume, oxygen molar volume and oxygen packing density were determined. Glasses are characterized with high glass transition temperature. Raman analysis revealed that the glass structure is built up mainly from tetrahedral $(MoO_4)^{2-}$ and $(WO_4)^{2-}$ units providing Raman bands of around 317 cm^{-1}, 341-352 cm^{-1}, 832-820 cm^{-1} and 928-935 cm^{-1}. At the same time with the replacement of MoO_3 with WO_3 some fraction of WO_6 octahedra are produced, which number increases with the increasing WO_3 content. A strong red emission from the $^5D_0$ level of Eu^{3+} ions was registered under near UV (395 nm) excitation using the $^7F_0 \rightarrow {}^5L_6$ transition of Eu^{3+}. PL emission gradually increases with increasing WO_3 content evidencing that WO_3 is more appropriate component than MoO_3. The integrated fluorescence intensity ratio R ($^5D_0 \rightarrow {}^7F_2/{}^5D_0 \rightarrow {}^7F_1$) was calculated to estimate the degree of asymmetry around the active ion, suggesting a location of Eu^{3+} in non-centrosymmetric sites.

Keywords: glasses; structure; europium; photoluminescence

1. Introduction

Trivalent europium doped materials are usually considered as good red-emitting phosphor candidates for LEDs. Its characteristic energy transfer generates a strong emission with a high color purity [1]. Unfortunately,Eu^{3+}-doped materials cannot be efficiently excited by the present LED chips, because its excitation peaks are weak in nature due to parity-forbidden f–f transitions [2]. The use of the inorganic host matrices with strong absorption in the ultraviolet (UV) region, which occurs commonly via excitation under Ligand-to-Metal Charge Transfer (LMCT) absorption bands, is a usual approach to improve the luminescence intensities from the Eu^{3+} materials [3]. Among many inorganic compounds, molybdates and tungstate phases are widely studied for decades as hosts for lanthanide doping due to their absorption in the mid ultraviolet region via O(2p) → W(5d)/Mo(4d) charge transfer and subsequent transfer of the energy to the low-lying emissive states of trivalent lanthanide ions [3,4]. At the present, the reports are mainly focused on the preparation of the

 doi:10.20944/preprints202409.0145.v1

crystalline molybdate and tungstate host structures, while data for the molybdate and tungstate glass and glass ceramic rare earth hosts are limited [1–16]. Compared with bulk crystalline hosts, glasses have the advantages of easy fabrication, low cost, high mechanical strength, and high chemical durability. Therefore, it is meaningful to prepare molybdate and tungstate glass compositions doped with rare earth activators and to investigate their luminescence.

In our previous works we have reported the preparation of Eu^{3+} doped glasses and glass ceramics with a high WO_3 content in the systems WO_3:La_2O_3:B_2O_3 and WO_3:La_2O_3:B_2O_3:Nb_2O_5 possessing strong 613 nm red luminescence with excitation at 390 nm, that is an indication they could be promising materials for red-light source. [17,18]. In our more recent works, we have obtained tungsten-containing ZnO–B_2O_3 glasses doped with Eu^{3+} active ion and we have studied their luminescent properties [19–21]. The obtained results from glass structure, physical, thermal, and optical properties indicate the suitability of the 50ZnO:40B_2O_3:10WO_3 glass network for the luminescence performance of Eu^{3+} ions. The positive effect of the addition of WO_3 on the luminescence intensity is proven by the stronger Eu^{3+} emission of the zinc–borate glass containing WO_3 compared to the WO_3-free zinc–borate glass, a phenomenon engendered mainly by the energy transfer from tungstate groups to the Eu^{3+} ions (sensitizing effect). The most intense luminescence peak observed at 612 nm and the high-integrated emission intensity ratio (R) of the $^5D_0 \rightarrow {}^7F_2$/ $^5D_0 \rightarrow {}^7F_1$ transitions at 612 nm and 590 nm of 5.77 suggest that the glasses have the potential for red emission materials. We have also prepared a homogeneous optically transparent ternary MoO_3-La_2O_3-B_2O_3 and WO_3-La_2O_3-B_2O_3 glasses containing a large amount of MoO_3 (10-50 mol%) and WO_3 (15 – 50 mol%) and as well as quaternary glasses with nominal compositions of (50-x)MoO_3:xWO_3:25La_2O_3:25B_2O_3, x = 0, 10, 20, 30, 40, 50 mol% and we have investigated their structure and crystallization behavior [22-24]. It was proposed that the glass structure of ternary and quaternary glasses is built up mainly from tetrahedral $(MoO_4)^{2-}$ and $(WO_4)^{2-}$ units and BO_3 and BO_4 groups. The main crystalline phases in the crystallized MoO_3-La_2O_3-B_2O_3 glasses were found to be $LaMoBO_6$ and LaB_3O_6. The formation of $LaMo_{x-1}W_xO_6$ solid solutions was confirmed in the crystallized samples from MoO_3-WO_3-La_2O_3-B_2O_3 system.

In this paper we continue our investigations over glasses in the MoO_3-WO_3-La_2O_3-B_2O_3 system. The purpose is to obtained Eu^{3+} doped glasses with nominal compositions of (50-x)MoO_3:xWO_3:25La_2O_3:25B_2O_3:3Eu^{3+}, x = 0, 10, 20, 30,40,50 mol% and to study their thermal behavior, structure and luminescent properties.

2. Results and Discussion

2.1. Thermal analysis

The DTA curves of the (50-x)MoO_3:xWO_3:25La_2O_3:25B_2O_3:3Eu^{3+}, x= 0, 10, 20, 30, 40, 50 mol% glasses are shown on Figure 1.

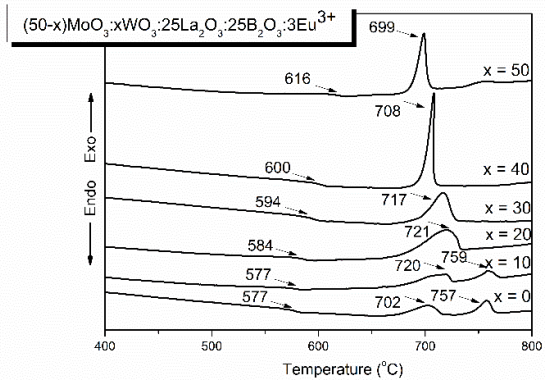

Figure 1. DTA curves of (50-x)MoO_3:xWO_3:25La_2O_3:25B_2O_3:3Eu^{3+}, x= 0, 10, 20, 30, 40, 50 mol% glasses.

 doi:10.20944/preprints202409.0145.v1

The endothermic dips corresponding to the glass transition temperature (T_g) and the exothermic peaks due to the crystallization temperature (T_c) are observed. The values of T_g and T_c estimated are pointed out on the figure. As it is seen the glass transition temperature increase from 577 °C to 616 °C with the substitution of WO_3 for MoO_3 because of the replacement of weaker Mo-O bonds with a stronger W-O bonds [24]. In the DTA curves of glasses with a higher MoO_3 content (x = 0 and x = 10) two broad exothermic peaks are observed, while glasses with a higher WO_3 content (x = 50 and x= 40) are characterized with one sharp and intensive exothermic effect, evidencing different crystallization behavior depending on the compositions. The x = 0 glass has higher thermal stability against crystallization i. e. $\Delta T = T_c - T_g$ = 125 °C compared to the ΔT of x =50 glass (83°C) evidencing better glass forming ability of molybdate than tungstate glass. On the other hand glasses containing higher amount of MoO_3 and lower WO_3 content up to 20 mol% have the highest ΔT values (145°C for glass x = 10 and 137°C for glass x= 20), indicating that the addition of a small amount WO_3 into the molybdate glass improves glass formation tendency of the compositions.

2.2. Structural investigations

2.2.1. Raman analysis

Raman spectra of (50-x) MoO_3:xWO_3:25La_2O_5:25B_2O_3:3Eu^{3+} (x=0, 10, 20, 30, 40, 50 mol%) glasses are shown in Figure 2. All spectra consist of broad Raman bands at around 317 cm^{-1}, 341-352 cm^{-1}, 832-820 cm^{-1} and 928-935 cm^{-1}. The spectra obtained are similar with the spectra of four component glasses (50-x)MoO_3:xWO_3:25La_2O_5:25B_2O_3 , x=10, 20, 30, 40, 50 and three component xMoO_3:25La_2O_3:(75-x)B_2O_3, x= 10-50 and xWO_3:25La_2O_3:(75-x)B_2O_3, x=15, 25, 50 glasses previously reported and discussed by us in detail in the ref [22–24].

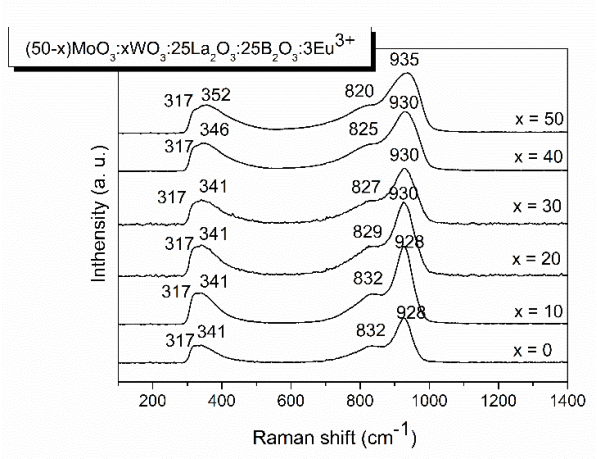

Figure 2. Raman spectra of (50-x)MoO_3:xWO_3:25La_2O_3:25B_2O_3:3Eu^{3+}, x= 0, 10, 20, 30, 40, 50 mol% glasses.

Based on these former data, we can assigned the Raman bands obtained as follows. The most intense band at 928-935 cm^{-1} is ascribed to the symmetric stretching vibration mode ν_1 of isolated $(MoO_4)^{2-}$ and $(WO_4)^{2-}$ tetrahedral units. As it is seen from the Figure 2, this band became broader with an increasing WO_3 content. Spectral deconvolution performed in ref. [22–24] has shown the presence of weak band at 980-996 cm^{-1} related to WO_6 octahedral groups in WO_3-containing glasses. The band at 832-820 cm^{-1} is due to the asymmetric ν_3 stretching vibration of $(MoO_4)^{2-}$ and $(WO_4)^{2-}$ groups. Two Raman bands at low frequency spectral region at 315 $cm^{-1}$and 341-352 $cm^{-1}$are interpreted as the symmetric bending mode ν_2 of $(MoO_4)^{2-}$ and $(WO_4)^{2-}$ tetrahedral units, that overlap with the Eu-O vibration and vibration of LnO_n units respectively [20,22–24]. In the Raman spectra obtained there are no any peaks in the region of 1000-1500 cm^{-1}, where Raman bands of the boron oxygen groups are situated [20]. However, having in mind our previous works over similar glass compositions [22–

 doi:10.20944/preprints202409.0145.v1

24], it could be suggested that BO_3 and BO_4 groups and B-O-B bonds are also present in the structure of the investigated glasses. The spectral results obtained suggest that the structure of (50-x)MoO_3:xWO_3:25La_2O_5:25B_2O_3:3Eu^{3+} (x=0, 10, 20, 30, 40, 50 mol%) glasses consists of mainly $(MoO_4)^{2-}$ and $(WO_4)^{2-}$ tetrahedral units which fraction changes continuously with the substitution of WO_3 for MoO_3. At the same time with the replacement of MoO_3 with WO_3 some amount of WO_6 octahedra are produced, which number increases with the increasing WO_3 content.

2.2.2. Physical parameters

A structural information of glasses was also gain by density (ϱ_g) measurement on which base the values of several physical parameters as: molar volume (V_m), oxygen molar volume (V_o) and oxygen packing density (OPD) are evaluated, using the following relations:

$$V_m = \frac{\Sigma x_i M_i}{\rho_g} \quad (1)$$

$$V_o = V_m \times \left(\frac{1}{\Sigma x_i n_i}\right) \quad (2)$$

$$OPD = 1000 \times C \times \left(\frac{\rho_g}{M}\right) \quad (3)$$

where x_i is the molar fraction of each component i, M_i the molecular weight, ϱ_g the glass density and n_i is the number of oxygen atoms in each oxide, C is the number of oxygen per formula units, and M is the total molecular weight of the glass compositions. The values obtained are listed in Table 1. As it is seen from the table, the density increases with the increasing WO_3 content at the expense of MoO_3 because of the replacement of lighter MoO_3 (molecular weight 143.94 g/mol) with heavier WO_3 (molecular weight 231.84 g/mol). The V_m and V_o values of glasses decrease, while their OPD values become greater with the gradual replacement of MoO_3 with WO_3 evidencing better packing and bonding in the glass network, with the introduction of WO_3 [25].

Table 1. Values of physical parameters of glasses (50-x)MoO_3:xWO_3:25La_2O_3:25B_2O_3:3Eu^{3+}, x=10, 20, 30, 40, 50 mol%: density (ϱ_g), molar volume (V_m), oxygen molar volume (V_o), oxygen packing density (OPD), Optical band gap (E_g), absorption edge A, refractive index, n.

Sample ID	ϱ_g (±0.01) (g/cm³)	V_m (cm³/mol)	V_o (cm³/mol)	OPD (g atom/l)	E_g direct (eV)	E_g indirect (eV)	A (nm)	Refractive index, n
x = 0	4.756	38.14	12.34	81.02	3.50	3.31	350.7	1.93144
x = 10	4.992	38.10	12.33	81.10	3.37	3.12	367.2	1.93452
x = 20	5.439	36.58	11.84	84.47	3.39	3.16	364.1	1.94278
x = 30	5.729	36.26	11.73	85.22	3.43	3.19	359.8	1.95236
x = 40	6.064	35.71	11.56	86.53	3.46	3.27	353.7	1.96115
x = 50	6.403	35.19	11.39	87.81	3.66	3.50	334.7	1.97066

It was found in our earlier paper that WO_6 and W-O-W bridging bonds are formed in the glass network of (50-x)MoO_3:xWO_3:25La_2O_3:25B_2O_3 , x=10, 20, 30, 40, 50 and xWO_3:25La_2O_3:(75-x)B_2O_3, x= 15, 25, 50 glasses [23,24]. The presence of bridging oxygens generates more connected glass structure, resulting in increase in the density and OPD and decrease in molar volume observed. The almost linear relationship between the density, physical parameters established and WO_3 content suggests

 doi:10.20944/preprints202409.0145.v1

an increasing number of WO_6 and their gradual polymerization (i. e. formation of W-O-W bonds) with WO_3 loading.

2.2.3. Optical studies

The optical absorption spectra at room temperature of (50-x) MoO_3:xWO_3:25La_2O_5:25B_2O_3:3Eu^{3+} (x=0, 10, 20, 30, 40, 50 mol%) glasses are shown in Figure 3. The absorption edge of ternary glasses, containing only MoO_3 or WO_3 (x = 0 and x = 50 respectively) shifts to the lower wavelength value in the UV range as compared with glasses containing both MoO_3 and WO_3. For instance, the absorption edge of glass x = 50 is 334. 7 nm, while for x = 10 the value of the absorption edge shifts to the 364.2 nm.

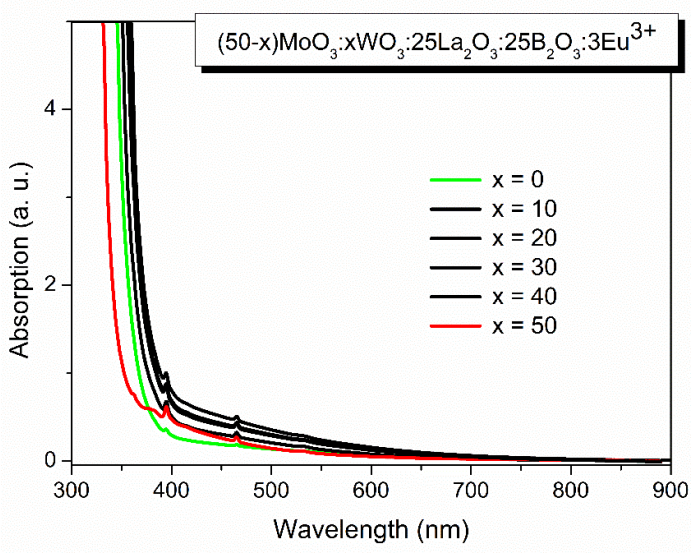

Figure 3. Optical absorption spectra at room temperature of (50-x)MoO_3:xWO_3:25La_2O_3:25B_2O_3-3Eu^{3+}, x= 0, 10,20, 30, 40, 50 mol% glasses.

The refractive index (n) for the presented glasses is also established from the optical absorption spectra. It is found that the refractive index increases with the increasing WO_3 content indicating the more densely packed structure in the presence of tungsten [26].

Some structural information also can be obtained from the optical band gap values (E_g) evaluated from the UV-Vis spectra with the Tauc method by plotting $(F(R_\infty)\ h\nu)^n$, where n = 0.5 or 2 for direct or indirect transition versus hν (incident photon energy), as shown in Figure 4, a, b and in Table 1 [27]. As it is seen from the Table 1, the E_g values of glasses containing both MoO_3 and WO_3, increases with the increasing WO_3 content due to an increase of the bridging W – O – W bonds concentration as a result of the accumulation of WO_6 structural units and their gradual polymerization [28]. This result coincide well with the variation in the physical parameters established. On the other hand E_g value of the molybdate glass x= 0 is lower than that of tungstate glass x = 50 evidencing the higher number of non-bridging oxygen species in the structure of glass x = 0 since it is accepted that in metal oxides, the creation of non-bonding orbitals with higher energy than bonding ones shifts the valence band to higher energy, which results in E_g decreasing [29].

 doi:10.20944/preprints202409.0145.v1

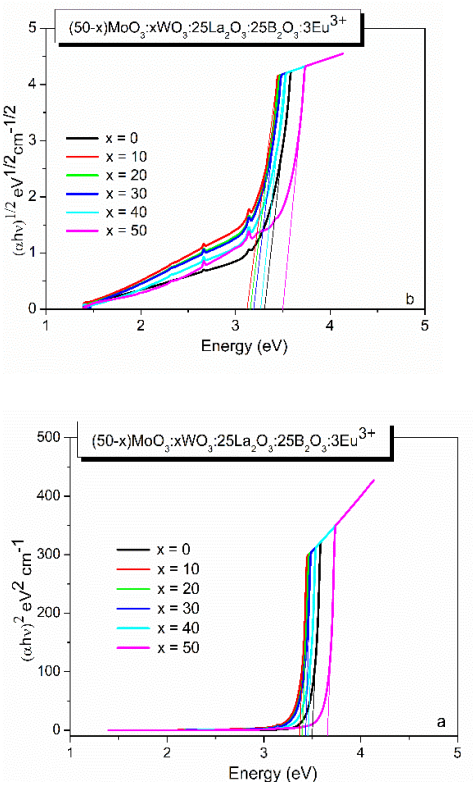

Figure 4. Tauc plot of (50-x)MoO_3:xWO_3:25La_2O_3:25B_2O_3:3Eu^{3+}, x= 0, 10, 20, 30, 40, 50 mol% glasses: a) for direct transition, b) for indirect transition.

To summarize this section,the Raman data obtained and as well as the established values of the structurally sensitive physical parameters demonstrate that the structure of (50-x) MoO_3:xWO_3:25La_2O_5:25B_2O_3:3Eu^{3+} (x=0, 10, 20, 30, 40, 50 mol%) glasses consists of mainly $(MoO_4)^{2-}$ and $(WO_4)^{2-}$ tetrahedral units which fraction changes continuously with the substitution of WO_3 for MoO_3. BO_3, BO_4 groups and B-O-B bonds also exist in the glass networks. Also with the replacement of MoO_3 with WO_3 some amount of WO_6 octahedra are produced, which number increases with the increasing WO_3 content. The WO_6 octahedra gradually polymerase forming W-O-W bonds with the increasing WO_3 content. Thus with the substitution of MoO_3 with WO_3 more disordered and connected glass structure is formed which is favorable for doping with Eu^{3+} active ions. DTA analysis also shows the increasing values of glass transition temperatures with the increasing WO_3 concentration confirming the formation of more connected and stable glass networks.

2.3. Luminescent properties

The photoluminescence excitation (PLE) spectra of the Eu^{3+} doped glasses are displayed in Figure 5. All data were obtained at room temperature by monitoring the most intensive characteristic emission of Eu^{3+} ions at 613 nm wavelength, corresponding to $^5D_0 \rightarrow {}^7F_2$ transition. From Figure 5 it can be observed that the PLE spectra consist of broad continuous band ranging from 220 to 350 nm and narrow - peaks in 350 - 600 nm wavelength range. Generally, the excitation broadband in the ultraviolet region arises due to the ligand - to - metal charge transfer (LMCT) from O^{2-} ligand to W^{6+}/Mo^{6+} ions in WO_n groups (WO_n = WO_4 and WO_6) and MoO_n groups (MoO_n = MoO_4) of the glass matrix as well as from O^{2-} ions to Eu^{3+} ions, i.e. electron transfer from the 2p orbital of O^{2-} to the empty 4f orbital of Eu^{3+} [30–34]. As it is seen from the Figure 5, in the PLE spectrum of the glass x = 50, two maxima of the LMCT band are observed – one at about 260 nm and the other at about 325 nm. Considering the previous assignements of PLE peaks of Eu^{3+} ions [34,35], the bands at around 260 nm and 325 nm in the excitation spectra obtained would be assigned mainly to the $O^{2-} \rightarrow Eu^{3+}$ and O^{2-}

 doi:10.20944/preprints202409.0145.v1

→W^{6+}/Mo^{6+} LMCT transitions, respectively.The stronger intensity of the band at around 260 nm compared to the band at around 325 nm suggests that the O^{2-}→ Eu^{3+} LMCT is taking place largely in the glass x = 50.

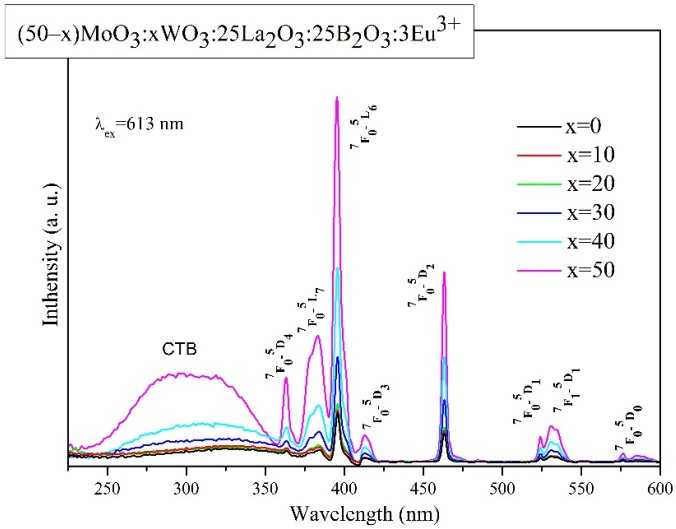

Figure 5. Excitation spectra of (50–x)MoO_3:xWO_3:25La_2O_3:25B_2O_3:3Eu^{3+} (x = 0, 10, 20, 30, 40 and 50 mol%) glasses.

The presence of the excitation band of MoO_n and WO_n groups, recorded at the emission wavelength of Eu^{3+} at 613 nm suggests the existence of non - radiative energy transfer from glass matrix to the active rare earth ion [34,36]. As can be seen, the intensity of this band highly depends on the WO_3 concentration and increases with the increasing of WO_3 content, suggesting that the energy transitions O^{2-} → W^{6+}, in comparison to O^{2-} → Mo^{6+}, largely influence the intensity of the charge transfer absorption band of host matrix. Thus, it can be assumed that WO_3 will contribute predominantly to the non - radiative energy transfer to the Eu^{3+} active ions and the glasses containing significant tungsten oxide concentrations will exhibit the most intense emission. This process is known as host sensitized luminescence.

The excitation spectra also show several peaks between 350 - 600 nm wavelength range, assigned to the f - f intra - configurational forbidden transitions of Eu^{3+} from the ground state ($^7F_0$) and from the first excited state ($^7F_1$): $^7F_0$ → $^5D_4$ (363 nm), $^7F_1$ → $^5L_7$ (383 nm), $^7F_0$ → $^5L_6$ (395 nm), $^7F_0$ → $^5D_3$ (412 nm), $^7F_0$ → $^5D_2$ (463 nm), $^7F_0$ → $^5D_1$ (523 nm), $^7F_1$ → $^5D_1$ (531 nm) and $^7F_0$ → $^5D_0$ (577 nm) [37], of which the $^7F_0$ → $^5L_6$ (395 nm) transition is the most intensive and was considered as an excitation wavelength to record the emission spectra. Compared to the LMCT, the f - f transitions are stronger and their intensity increases, as the concentration of WO_3 increases, which is advantageous for achieving appropriate excitation by near - UV and blue LED chips, since in general the intensity of these Eu^{3+} transitions is weak due to the fact that they are forbidden by the Laporte`s selection rule [38].

The photoluminescence emission (PL) spectra of Eu^{3+} - doped glasses, recorded under the most intensive Eu^{3+} excitation at 395 nm light are shown in Figure 6. The characteristic emission peaks originated from the radiative transitions of Eu^{3+} ions from the $^5D_0$ excited state to the lower - lying $^7F_0$, $^7F_1$, $^7F_2$, $^7F_3$, $^7F_4$ ground states are observed at 580 nm, 593 nm, 613 nm, 652 nm and 702 nm, respectively. The dominant luminescent band is located at 613 nm. From Figure 6 it is clear that the emission intensity strongly depends on the WO_3 concentration and increases considerably as its content increases. This observation may be due to the occurring non-radiative charge transfer from glass host to the active Eu^{3+} ion. Evidence for the existence of the energy transfer is the absence of the characteristic broad emissions of WO_3 and MoO_3 in the spectral range 400 - 600 nm [39,40] arising from the fact that the energy absorbed by the tungstate and molybdate groups has transferred non - radiatively to the active Eu^{3+} ion.

 doi:10.20944/preprints202409.0145.v1

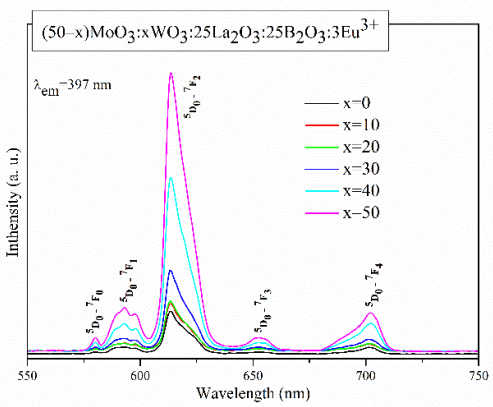

Figure 6. Emission spectra of (50–x)MoO_3:xWO_3:25La_2O_3:25B_2O3:3Eu^{3+} (x = 0, 10, 20, 30, 40 and 50 mol%) glasses.

Among all the observed emission transitions, $^5D_0 \rightarrow {}^7F_2$ transition is identified as electric dipole (ED) and is forced by the crystal field environment in the vicinity of the Eu^{3+} ions, while $^5D_0 \rightarrow {}^7F_1$ transition is allowed magnetic dipole (MD) in nature, independent of host matrix.

When Eu^{3+} ions are embedded in sites with inversion symmetry, the $^5D_0 \rightarrow {}^7F_1$ magnetic dipole transition will dominate; on the contrary, when a Eu^{3+} ion site is noncentrosymmetric, the $^5D_0 \rightarrow {}^7F_2$ electric dipole transitions will be the strongest in the emission. As a result, the luminescence intensity ratio (R) between electric ($^5D_0 \rightarrow {}^7F_2$) and magnetic ($^5D_0 \rightarrow {}^7F_1$) dipole transitions can be used as a probe to the nature of the site and symmetry of the coordination sphere and provide valuable information about the local symmetry around the rare earth ion, the strength of covalent bonding between Eu^{3+} and its surrounding ligands and the emission intensity. The higher the value of R, the more distortion from inversion symmetry is observed, as well as higher covalency between Eu^{3+} and O^{2-} ions and increased emission intensity [37,41,42]. The calculated intensity ratios R (7.09-7.82) of the obtained glasses (Table 2) are higher than those of previously synthesized by us glasses [20,43–46] and than other Eu^{3+} doped oxide glasses reported in literature [47–53], as well as the commercially available red phosphors Eu^{3+}:Y_2O_3 [54,55] and Eu^{3+}:Y_2O_2S [56] suggesting that the synthesized samples are characterized with more asymmetry in the vicinity of Eu^{3+} ions, stronger Eu - O covalence, and an enhanced emission intensity. From Table 2 it also could be seen that, the value of asymmetric ratio is increasing as the WO_3 content increases and as a result stronger luminescence is observed.

Table 2. Relative luminescent intensity ratio (R) of the two transitions ($^5D_0 \rightarrow {}^7F_2$)/($^5D_0 \rightarrow {}^7F_1$) for (50-x)MoO_3:xWO_3:25La_2O_3:25B_2O_3 :3Eu^{3+} (x = 0, 10, 20, 30, 40 and 50 mol%) glasses.

Glass composition	Relative Intensity Ratio, R	reference
50MoO_3:25La_2O_3:25B_2O_3:3Eu_2O_3	7.09	Current work
40MoO_3:10WO_3:25La_2O_3:25B_2O_3:3Eu_2O_3	7.15	Current work
30MoO_3:20WO_3:25La_2O_3:25B_2O_3:3Eu_2O_3	7.19	Current work
20MoO_3:30WO_3:25La_2O_3:25B_2O_3:3Eu_2O_3	7.42	Current work
10MoO_3:40WO_3:25La_2O_3:25B_2O_3:3Eu_2O_3	7.63	Current work
50WO_3:25La_2O_3:25B_2O_3:3Eu_2O_3	7.82	Current work

 doi:10.20944/preprints202409.0145.v1

$50ZnO:40B_2O_3:10WO_3:xEu_2O_3$ ($0 \le x \le 10$)	4.54÷5.77	20
$50ZnO:40B_2O_3:5WO_3:5Nb_2O_5:xEu_2O_3$ ($0 \le x \le 10$)	5.09÷5.76	43
$50ZnO:(50–x)B_2O_3:xNb_2O_5:0.5Eu_2O_3$:, x= 0, 1, 3 and 5 mol%	4.31-5.16	44
$50ZnO:(50–x)B_2O_3:0.5Eu_2O_3:xWO_3$, x = 0, 1, 3, 5.	4.34-5.57	45
50ZnO:(49–x)B2O3:1Bi2O3:xWO3; x = 1, 5, 10,	4.61-5.73	46
$4ZnO:3B_2O_3$ 0.5–2.5 mol % Eu_2O_3	2.74-3.94	47
$60ZnO:20B_2O_3:(20 - x)SiO_2–xEu_2O_3$ (x = 0 and 1)	3.166	48
$15PbF_2:25WO_3:(60–x)TeO_2:xEu_2O_3$ x = 0.1, 0.5, 1.0 and 2.0 mol%	2.37-2.78	49
$20PbO–5CaO–5ZnO–10LiF–59B_2O_3–1Eu_2O$	2.320	50
$45SiO_2–(20–x)PbF_2–20K_2O–5Na_2O–10LiF–1.0Eu_2O_3$	2.44	51
$89.5B_2O_3–10Li_2O–0.5Eu_2O_3$	2.41	52
$57GeO_2–40K_2O–3Eu_2O_3$	3.70	52
$73P2O5–25CaO–2Eu_2O_3$	3.95	52
$79TeO_2–20Li_2CO_3–1Eu_2O_3$	4.28	53
$Eu^{3+}:Y_2O_3$	3.8-5.2	54, 55
$Eu^{3+}:Y_2O_2S$	6.45-6.62	56

Additional evidence of the low site symmetry in the vicinity around the active Eu^{3+} ions is the presence of the $^5D_0 \rightarrow {}^7F_0$ transition, which is strictly forbidden and according by Binnemans, appears in emission spectra when Eu^{3+} ions are located in sites with C_{2v}, C_n or C_s symmetry [37]. To further examine the symmetry of the Eu^{3+} sites, the $^5D_0 \rightarrow {}^7F_1$ transition is considered, which displays splittings. This implies that the symmetry of the Eu^{3+} sites in the studied glasses are C_{2v} or lower [57].

The observed optical properties are discussed on the basis of the glass structural features. The most intensive Eu^{3+} emission peak, corresponding to the hypersensitive $^5D_0 \rightarrow {}^7F_2$ transition, along with the high values of the luminescent ratio R, evidence that Eu^{3+} ions are located in low site symmetry in the host matrix. This emission peak intensity and the R values of investigated glasses increases with the increasing WO_3 concentration indicating that the substitution of MoO_3 with WO_3 contributes to the creation of a more distorted and rigid glass structure that lowers the site symmetry of the rare-earth ion and improves its photoluminescence behavior. Furthemore, the increasing intensity of the band at 613 nm ($^5D_0 \rightarrow {}^7F_2$ transition) with increasing WO_3 concentration indicates that the WO_3 contributes predominantly to the non - radiative energy transfer to the Eu^{3+} active ions (host sensitized luminescence). Thus, WO_3 is more appropriate component than MoO_3 for enhancing the luminescent intensity of the doped Eu^{3+} ion.

 doi:10.20944/preprints202409.0145.v1

3. Materials and Methods

The glasses with the nominal compositions of (50-x)MoO_3:xWO_3:25La_2O_3:25B_2O_3:3Eu^{3+} , x=10, 20, 30, 40, 50 (mol%) were prepared using a conventional melt quenching method. Reagent grade commercial powders of MoO_3, WO_3, La_2O_3, and H_3BO_3, were used as starting materials and were mixed in an alumina mortar. The batches (each batch weight:10 g) were melted at 1200-1250°C for 30 min in a platinum crucible in air. The glasses were obtained by pouring the melts onto an iron plate and by pressing with another iron plate (cooling rate ~ 10 K/s). The glass transition (T_g) and crystallization peak (T_c) temperatures were determined using differential thermal analysis (DTA) (Rigaki Thermo Plus TG 8120) at heating rate of 10 K/min (±1). Optical absorption spectra at room temperature of glasses were measured in the wavelength range of 200-800 nm using a spectrometer (Shimadzu U-3120). The uncertainty in the observed wavelength is about ±1 nm. Refractive indices at a wavelength (λ) of 632.8 nm (He–Ne laser) were measured at room temperature with a prism coupler (Metricon Model 2010). Densities of the glasses at room temperature were determined with the Archimedes method using distilled water as an immersion liquid in which measurements were repeated five times and the average value was used (±0.001g/cm^3). Raman scattering spectra at room temperature were measuresd with a laser microscope (Tokyi Instruments Co. Nanofinder) operated at Ar^+ (λ = 448 nm) laser with resolution of ±1 cm^{-1}. PL spectra at room temperature for the glass samples were measured with a PL spectrometer (JASCO FP-6500).

4. Conclusions

The glasses with nominal composition of (50-x)MoO_3:xWO_3:25La_2O_3:25B_2O_3 :3Eu^{3+} (x = 0, 10, 20, 30, 40 and 50 mol%) were synthesized by melt quenching method and their structure, thermal behavior and luminescent properties were studied. The glass transition temperature increases with the substitution of MoO_3 with WO_3. Glasses containing higher amount of MoO_3 and lower WO_3 content up to 20 mol% have the highest thermal stability (ΔT = 145°C for glass x = 10 and ΔT =137°C for glass x= 20). On the base of Raman analysis and as well as density measurements and values of the structurally sensitive physical parameters it was established that the glass structure is build up mainly from $(MoO_4)^{2-}$ and $(WO_4)^{2-}$ tetrahedral units. WO_6 octahedral groups and W-O-W bonds are also formed in the WO_3-containing glasses, increasing in number with an increase of WO_3 content. The luminescent properties of the obtained Eu^{3+} - doped glasses revealed that they could be excited by 395 nm and exhibit pure red emission centered at 613 nm ($^5D_0 \rightarrow {}^7F_2$ transition). The Eu^{3+} luminescent intensity were found to increase with the WO_3 loading. All findings obtained here are favorable for the elaboration of novel red-emitting glass materials.

Author Contributions: Conceptualization, R.I. A.Y. and L.A; methodology, L.A. K.S. T.H. and T.K; software, L.A. K. S. and T. H.; validation, R.I. and L.A; formal analysis, R.I. A.Y. and L.A; investigation, L.A. K. S. and T. H.; resources, L.A. K. S. T. H. and T. K; data curation, R.I. and T. K; writing—original draft preparation, A.Y. and M. M.; writing—review and editing, R.I. K.S. T.H. and T.K; visualization, R.I. A.Y. and L.A; supervision, R.I. T.K. and L.A; project administration, L.A.; funding acquisition, L.A. All authors have read and agreed to the published version of the manuscript.

Funding: This research received no external funding.

Informed Consent Statement: Not applicable.

Data Availability Statement: Data are contained within the article.

Conflicts of Interest: The authors declare no conflicts of interest.

References

1. Kim, J.; The Role of Auxiliary Alkali Metal Ions on Scheelite Structure Double Molybdate and Tungstate Phosphors. Inorg. Chem. **2017**, 56, 8078−8086
2. Janulevicius, M.; Marmokas, P.; Misevicius, M.; Grigorjevaite, J.; Mikoliunaite, L.; Sakirzanovas, S.; Katelnikovas, A. Luminescence and luminescence quenching of highly efficient $Y_2Mo_4O_{15}$:Eu^{3+} phosphors and ceramics. *Scientific Reports* **2016**, *6*, 26098.

 doi:10.20944/preprints202409.0145.v1

3. Moreira, R.; Francisco, L.; Costa, I.; Barbosa, H.; Teotonio, E.; Felinto, M.; Malta, O.; Brito, H. Luminescence properties of $BaMO_4:Eu^{3+}$ (M: Mo or W) phosphors derived from co-precipitation reaction. *J. Alloys Compd.* **2023**, *937*, 168408.
4. Dutta, P. S.; Khanna, A. Eu^{3+} activated molybdate and tungstate based red phosphors with charge transfer band in blue region. *ECS J. Solid State Sci. Technol.* **2013**, 2, R3153-R3167.
5. Yengkhom, D.; Ningombam, G.; Singh, T.; Chipem, F.; Singh N.; Luminescence enhancement and tunable color emission in Eu/Dy/Sm codoped $CaW_{1-x}Mo_xO_4$ phosphor. *Inorg. Chem. Commun*. **2022**, *141*, 109571.
6. Pier, T.; Jüstel, T.; Application of Eu(III) activated tungstates in solid state lighting. *Opt. Mater.: X*, **2024**, *22*, 100299.
7. Vatsa B.; Shafeeq, M.; Kesari, Swayam. Triple molybdates and tungstates scheelite structures: Effect of cations on structure, band-gap and photoluminescence properties. *J. Alloys Compd.* **2021**, *865*, 158818.
8. Zhang, W.J.; Feng, W.L.; Nie, Y.M., Photoluminescence properties of red europium doped calcium tungstate phosphors for blue-pumped light-emitting diodes. *Optik*, **2015**, *126*, 1341-1343.
9. Czajka, J.; Szczeszak, A.; Kaczorowska, N.; Lis, Stefan. New Multicolor Tungstate-Molybdate Microphosphors as an Alternative to LED Components. *Materials* **2021**, *14*, 6608.
10. Wang, Y.; Honma, T.; Doi, Y.; Hinatsu, Y.; Komatsu,T. Magnetism of β′-$Gd_2(MoO_4)_3$ and photoluminescence of β′-$Eu_2(MoO_4)_3$ crystallized in rare-earth molybdenum borate glasses. *J. Ceram. Soc. Jpn.* **2013**, *121*, 230-235.
11. Devi, C.h.B.Annapurna.; Mahamuda, Sk.; Swapna, K.; Venkateswarlu, M.; Srinivasa Rao, A.; Vijaya Prakash, G. Compositional dependence of red luminescence from Eu^{3+} ions doped single and mixed alkali fluoro tungsten tellurite glasses. *Opt. Mater.* **2017**, *73*, 260–267.
12. Roy, J. S.; Messaddeq, Y. Photoluminescence study of Eu^{3+} doped zinc tungsten-antimonite glasses for red LED applications. *J. Lumin.* **2020**, *228*, 117608-4.
13. Wantana, N.; Kaewnuam, E.; Ruangtaweep, Y.; Kidkhunthod, P.; Kim, H.J.; Kothanf, S.; Kaewkhao, J.; High density tungsten gadolinium borate glasses doped with Eu^{3+} ion for photonic and scintillator applications. *Radiat. Phys. Chem.* **2020**, *172*, 108868-7.
14. Dousti, M.R.; Poirier, G.Y.; de Camargo, A.S.S. Tungsten sodium phosphate glasses doped with trivalent rare earth ions (Eu^{3+}, Tb^{3+}, Nd^{3+} and Er^{3+}) for visible and near-infrared applications. *J. Non-Cryst. Solids* **2020**, *530*, 119838-7.
15. Gandhi, Y.; Kityk, I. V.; Brik, M.G.; Raghav Rao, P.; Veeraiah, N. Influence of tungsten on the emission features of Nd^{3+}, Sm^{3+} and Eu^{3+} ions in ZnF_2–WO_3–TeO_2 glasses. *J. Alloys Compd.* **2010**, *508* 278–291.
16. Babu, A. M.; Jamalaiah, B.C.; Suhasini, T.; Srinivasa Rao, T.; Rama Moorthy, L. Optical properties of Eu^{3+} ions in lead tungstate tellurite glasses. *Solid State Sci.* **2011**, *13*, 574–578.
17. Aleksandrov, L.; Iordanova, R.; Dimitriev, Y.; Georgiev, N.; Komatsu, T. Eu^{3+} doped $1La_2O_3:2WO_3:1B_2O_3$ glass and glass-ceramic. *Opt. Mater.* **2014**, *36*, 1366-1372.
18. Milanova, M.; Aleksandrov, L.; Iordanova, R.; Petrova, P. A novel Eu^{3+}- doped tungstate glasses for red emission: preparation, structure and photoluminescence properties. *J. Chem. Technol. Metall.* **2022**, *57, 247-257*.
19. Milanova, M.; Aleksandrov, L.; Iordanova, R. Structure and luminescence properties of tungsten modified zinc borate glasses doped with Eu^{3+} ions. *Mater. Today: Proc*. **2022**, *61*, 1206-1211.
20. Milanova, M.; Aleksandrov, L.; Yordanova, A.; Iordanova, R.; Tagiara, N. S.; Herrmann, A.; Gao, G.; Wondraczek. L.; Kamitsos, E. I. Structural and luminescence behavior of Eu^{3+} ions in $ZnO-B_2O_3-WO_3$ glasses. *J. Non-Cryst. Solids* **2023**, *600*, 122006.
21. Yordanova, A.; Aleksandrov, L.; Milanova, M.; Iordanova, R.; Petrova, P.; Nedyalkov, N. Effect of WO_3 addition on the structure and luminescent properties of $ZnO-B_2O_3:Eu^{3+}$ glass, Molecules, **2024**, *29*, 2470.
22. Aleksandrov, L.; Komatsu, T.; Iordanova, R.; Dimitriev, Y. Study of molybdenum coordination state and crystallization behavior in MoO_3-La_2O_3-B_2O_3 glasses by Raman spectroscopy. *J. Phys. Chem. Solids* **2011**, *72*, 263-268.
23. Aleksandrov, L.; Komatsu, T.; Iordanova, R.; Dimitriev, Y. Raman spectroscopy study of WO_3-La_2O_3-B_2O_3 glasses with no color and crystallization of $LaBWO_6$, Opt. Mater. **2011**,34, 201-206.
24. Aleksandrov, L.; Komatsu, T.; Shinozaki, K.; Honma, T.; Iordanova, R. Structure of MoO_3-WO_3-La_2O_3-B_2O_3 glasses and crystallization of $LaMo_{1-x}W_xBO_6$ solid solutions. *J. Non-Cryst. Solids* **2015**, *429*, 171-177.
25. Villegas, M. A.; Fernández Navarro, J. M. Physical and structural properties of glasses in the TeO_2–TiO_2–Nb_2O_5 system. *J Eur Ceram Soc.* **2007**, *27*, 2715–2723.

26. Masuno, A.; Inoue, H.; Yoshimoto, K.; Watanabe, Y. Thermal and optical properties of La_2O_3 -Nb_2O_5 high refractive index glasses. Opt. Mater. Express **2014**, *4*, 710-717.
27. Tauc, J. Amorphous and Liquid Semiconductor; Plenum Press: London, UK; New York, NY, USA, **1974**.
28. Milanova, M.; Kostov, K.L.; Iordanova, R.; Aleksandrov, L.; Yordanova, A.; Mineva, T. Local structure, connectivity and physical properties of glasses in the B_2O_3- Bi_2O_3-La_2O_3-WO_3 system, J. Non-Cryst. Solids, **2019**, *516*, 35-44.
29. Rani, S.; Sanghi, S.; Ahlawat, N.; Agarwal, A. Influence of Bi_2O_3 on thermal, structural and dielectric properties of lithium zinc bismuth borate glasses. J. Alloys Compd. **2014**, 597, 110–118.
30. Blasse, G.; Grabmaier, B.C. *Luminescent Materials*, 1st ed.; Springer Berlin: Heidelber, Germany, **1994**; pp.18
31. Hoefdraad, H.E. The charge-transfer absorption band of Eu^{3+} in oxides. *J. Solid State Chem.* **1975**, *15(2)*, 175–177.
32. Parchur, A.K.; Ningthoujam, R.S. Behaviour of electric and magnetic dipole transitions of Eu^{3+}, $^5D_0 \rightarrow {}^7F_0$ and Eu–O charge transfer band in Li^+ co-doped YPO_4:Eu^{3+}. *RSC Adv.* **2012**, *2*, 10859-10868.
33. Mariselvam, K.; Juncheng L. Synthesis and luminescence properties of Eu^{3+} doped potassium titano telluroborate (KTTB) glasses for red laser applications. *J. Lumin.* **2021**, *230*, 117735.
34. Dutta, P.S.; Khanna, A. Eu^{3+} activated molybdate and tungstate based red phosphors with charge transfer band in blue region. *ECS J. Solid State Sci. Technol*. **2013,** *2*, R3153–R3167.
35. Kotaka, M.; Honma, T.; Komatsu, T. Photoluminescence features of new Eu^{3+} -doped $Gd_4Mo_7O_{27}$ phosphors synthesized using glass crystallization technique. *J. Asian Ceram. Soc.* **2018**, *6*, 314–321.
36. Thieme, C.; Herrmann, A.; Kracker, M.; Patzig, C.; H¨oche T.; Rüssel, C. Microstructure investigation and fluorescence properties of Europium-doped scheelite crystals in glass-ceramics made under different synthesis conditions. *J. Lumin.* **2021**, *238*, 118244.
37. Binnemans, K. Interpretation of europium(III) spectra. *Coord. Chem. Rev* **2015,** *295*, 1–45.
38. J. C. G. Bünzli, Lanthanide luminescence: from a mystery to rationalization, understanding, and applications, Handbook on the Physics and Chemistry of Rare Earths, Elsevier, **2016,** *50*, 141-176.
39. Sungpanich, J.; Thongtem, T.; Thongtem, S. Large-scale synthesis of WO_3 nanoplates by a microwave-hydrothermal method. *Ceram. Int.* **2012,** *38(2)*, 1051-1055
40. Song, J.; Ni, X.; Zhang, D.; Zheng, H. Fabrication and photoluminescence properties of hexagonal MoO_3 rods. *Solid State Sci.* **2006**, *8(10)*, 1164-1167.
41. Devi, C.H.B.; Mahamuda, S.; Swapna, K.; Venkateswarlu, M.; Rao, A.S.; Prakash, G.V. Compositional dependence of red luminescence from Eu^{3+} ions doped single and mixed alkali fluoro tungsten tellurite glasses. Opt. Mater. **2017**, *73*, 260–267.
42. Nogami, M.; Umehara, N.; Hayakawa, T. Effect of hydroxyl bonds on persistent spectral hole burning in Eu^{3+} doped BaO-P_2O_5 glasses. Phys. Rev. B **1998**, *58*, 6166–6171.
43. Aleksandrov, L.; Milanova, M.; Yordanova, A.; Iordanova, R.; Nedyalkov, N.; Petrova, P.; Tagiara, N.S.; Palles, D.; Kamitsos, E.I. Synthesis, structure and luminescence properties of Eu^{3+}-doped 50ZnO.40B_2O_3.5WO_3.5Nb_2O_5 glass. *Phys. Chem. Glas. Eur. J. Glass Sci. Technol. B* **2023**, *64*, 101-109.
44. Iordanova, R.; Milanova, M.; Yordanova, A.; Aleksandrov, L.; Nedyalkov, N.; Kukeva, R.; Petrova, P. Structure and Luminescent Properties of Niobium-Modified ZnO-B_2O_3:Eu^{3+} Glass. *Materials* **2024**, *17*, 1415.
45. Yordanova, A.; Aleksandrov, L.; Milanova, M.; Iordanova, R.; Petrova, P.; Nedyalkov, N. Effect of the Addition of WO_3 on the Structure and Luminescent Properties of ZnO-B_2O_3: Eu^{3+} Glass. *Molecules*, **2024,** *29(11)*, 2470.
46. Yordanova, A.; Milanova, M.; Iordanova, R.; Fabian, M.; Aleksandrov, L.; Petrova, P. Network Structure and Luminescent Properties of ZnO–B_2O_3–Bi_2O_3–WO_3: Eu^{3+} Glasses. *Materials.* **2023**, *16*(20), 6779.
47. Bettinelli, M.; Speghini, A.; Ferrari, M.; Montagna, M. Spectroscopic investigation of zinc borate glasses doped with trivalent europium ions. *J. Non-Cryst. Solids* **1996**, *201*, 211–221.
48. Annapurna, K.; Das, M.; Kundu, M.; Dwivedhi, R.N.; Buddhudu, S. Spectral properties of Eu^{3+}: ZnO–B_2O_3–SiO_2 glasses. *J. Mol. Struct.* **2005**, *741*, 53–60.
49. Babu, A.M.; Jamalaiah, B.C.; Suhasini, T.; Rao, T.S.; Moorthy, L.R. Optical properties of Eu3+ ions in lead tungstate tellurite glasses.*Solid State Sci.* **2011**, *13*, 574–578
50. Raju, B. D. P.; Reddy, C. M. Structural and optical investigations of Eu^{3+} ions in lead containing alkali fluoroborate glasses. *Opt. Mater*. **2012**, *34(8)*, 1251-1260.
51. Manasa, P.; Jayasankar, C. K. Luminescence and phonon side band analysis of Eu^{3+}-doped lead fluorosilicate glasses. *Opt. Mater*. **2016**, *62*, 139-145.

 doi:10.20944/preprints202409.0145.v1

52. Oomen E.W.J.L.; Dongen A.M.A. Europium (III) in oxide glasses: Dependence of the emission spectrum upon glass composition. *J. Non-Cryst. Solids* ***1989***, *111*, 205-213.
53. Kumar, A.; Rai, D. K.; & Rai, S. B. Optical studies of Eu3+ ions doped in tellurite glass. *Spectrochim Acta A Mol Biomol Spectrosc.* **2002**, *58(10)*, 2115-2125.
54. Song, H.; Chen, B.; Sun, B.; Zhang, J.; Lu, S. Ultraviolet light-induced spectral change in cubic nanocrystalline Y_2O_3: Eu^{3+}. *Chem. Phys. Lett.* **2003**, *372(3-4)*, 368-372.
55. Kabir, M.; Ghahari, M.; Afarani, M. S. Co-precipitation synthesis of nano Y_2O_3: Eu^{3+} with different morphologies and its photoluminescence properties. *Ceram. Int.* **2014**, *40(7)*, 10877-10885.
56. Som, S.; Mitra, P.; Kumar, V.; Kumar, V.; Terblans, J. J.; Swart, H. C.; Sharma, S. K. The energy transfer phenomena and colour tunability in Y_2O_2S: Eu^{3+}/Dy^{3+} micro-fibers for white emission in solid state lighting applications. *Dalton Trans.* **2014**, *43(26)*, 9860-9871.
57. Binnemans, K.; Görller-Walrand, C. Application of the Eu^{3+} ion for site symmetry determination. *J. Rare Earths* **1996**, *14*, 173–180.